physics

MDPI

Article

Applicability of Hydrodynamics in the Hadronic Phase of Heavy-Ion Collisions

Ronald Scaria, Captain R. Singh and Raghunath Sahoo *

Department of Physics, Indian Institute of Technology Indore (IITI), Simrol, Indore 453552, India; ronaldscaria.rony@gmail.com (R.S.); captainriturajsingh@gmail.com (C.R.S.)
* Correspondence: raghunath.sahoo@cern.ch

Abstract: The hadronic phase and its dynamics in relativistic heavy-ion collisions are topics of immense discussion. The hadronic phase contains various massive hadrons with an abundance of the lightest hadron, i.e., π-mesons (pions). In this paper, we consider that pions are in the thermal equilibrium in the hadronic phase and use second-order viscous hydrodynamics for a medium of massive pions to obtain its expansion to the boundary of the kinetic freeze-out. We achieve the kinetic freeze-out boundary with the Knudsen number Kn $>$ 1 limit. When this condition is met, hydrodynamics expansion breaks down, and the mean free path becomes sufficiently large in comparison with the system size so that the particle yields are preserved. Further, we investigate the effect of the massive fluid on the resonance particle yields, including re-scattering and regeneration, along with the natural decay widths of the resonances. The resonances can play an essential role in determining the characteristics of the hadronic phase as they have sufficiently small lifetimes, which may be comparable to the hadronic phase lifetime. In the current study, we predict the hadronic phase lifetime, which is further used to determine the $K^*(892)^0/K$, $\phi(1020)/K$, and $\rho(770)^0/\pi$ yield ratios at the kinetic freeze-out. We calculate these ratios as a function of charged particle multiplicity and transverse momentum and compare the findings with experimental data. Our calculations qualitatively agree with the experimental data, indicating a possible hydrodynamical evolution of the hadronic phase.

Keywords: heavy-ion collisions; hadronic phase lifetime; hydrodynamics; resonance production

check for updates

Received: 2 March 2025
Revised: 17 March 2025
Accepted: 27 March 2025
Published: 18 April 2025

Citation: Scaria, R.; Singh, C.R.; Sahoo, R. Applicability of Hydrodynamics in the Hadronic Phase of Heavy-Ion Collisions. *Physics* **2025**, *7*, 13. https://doi.org/10.3390/physics7020013

Copyright: © 2025 by the authors. Licensee MDPI, Basel, Switzerland. This article is an open access article distributed under the terms and conditions of the Creative Commons Attribution (CC BY) license (https://creativecommons.org/licenses/by/4.0/).

1. Introduction

Relativistic heavy-ion collisions provide a unique environment that encapsulates various phases of the QCD matter. The formation of a hot and dense, locally thermalized deconfined phase of colorful partons known as quark–gluon plasma (QGP) is expected to be formed in the very initial stages (proper time, $\tau < 1$ fm) following the collision. The emergence of a color-neutral hadronic phase ensues when the strongly interacting QGP phase dissipates, indicating a phase transition from a deconfined partonic phase to a colorless hadronic medium. Experimental data propose that the QGP phase exhibits behavior akin to those of a "perfect fluid" (PF) [1–4], characterized by exceptionally low shear viscosity (η) to entropy density (s) ratio near the AdS/CFT bound of $1/4\pi$ [5]. The QGP, formed at an extremely high initial temperature, is presumed to evolve based on hydrodynamic models before cooling down to the chemical freeze-out temperature. At this temperature, all inelastic collisions cease, leading to the breakdown of QGP hydrodynamics. Many of these computations are carried out assuming the QGP phase to be both chemically

and thermally equilibrated and composed of massless particles. The chemical freeze-out temperature closely aligns with the critical temperature (T_c) for phase transition predicted by lattice QCD (LQCD) calculations [6]. Using this framework, the lifetime of the QGP can be estimated in ultra-relativistic collisions [7,8]. However, defining the lifetime of the hadronic phase (the duration between chemical and kinetic freeze-outs) becomes somewhat ambiguous without an explicit definition of the kinetic freeze-out temperature or boundary.

Multiple models have been used to study the hadronic phase produced in relativistic nuclear collisions. One of the earliest studies describes [9] the hadronic phase as a system that is thermally equilibrated but chemically decoupled. This phase allows momentum transfer between the constituent particles through collisions. The calculations have been performed by assuming that the yields of resonances stay in equilibrium with those of the daughter particles formed from their decays. This assumption constitutes the concept of partial chemical equilibrium (PCE). It has been shown that the particle production in nuclear collisions can be assumed to be from a fireball following this partial chemical equilibrium approach [10]. This concept has been further used to determine the kinetic freeze-out temperature from the yields of hadrons and resonances [11]. Bayesian analysis of heavy ion data, on the other hand, has suggested that the particlization of the QGP phase occurs at about 150–160 MeV range [12–15], where both chemical and thermal equilibria are considered to break down. As this limit is obtained from relative particle yields, one can think of this as a limit on the chemical freeze-out. The hadronic phase thus produced is generally treated using transport models like the Ultra-relativistic Quantum Molecular Dynamics (UrQMD) model [16] or the AMPT (A Multi-Phase Transport) model [17]. These are generally used as afterburners to the hydrodynamic calculations, as in Refs. [18,19]. However, it has been observed that in such models, the intrinsic medium properties like viscosity are not well described [20,21]. For example, the hadronic evolution in UrQMD is shown to remember the prior QGP properties at hadronization [20] and can lead to different evolutions for different initial conditions chosen, although the final state properties are reproduced. This may be credited to the absence of an adequate definition of intrinsic transport properties in the UrQMD hadronic phase. Also, in Ref. [22], it has been shown that the hadronic evolution itself has transport properties comparable with a low viscous fluid. Recent advancements in far-from-equilibrium hydrodynamics [23,24] also imply the possibility of rapid thermalization even if the system is away from equilibrium. Therefore, employing hydrodynamics could thus be an alternate approach to describing the hadronic phase. Hydrodynamics treats the system as a continuous, locally thermalized fluid, which allows for the use of macroscopic properties like temperature, pressure, and flow velocity to describe the evolution of the medium. This approach is more effective at capturing the collective flow and the evolution of thermodynamic quantities, which are essential for understanding the bulk properties of the system. Additionally, hydrodynamic models can naturally incorporate concepts like PCE and provide a framework for determining the hadronic phase lifetime. By maintaining a thermalized description throughout the evolution, the hydrodynamic description of the hadronic phase may offer a consistent depiction of the hadronic phase.

In this direction, the Knudsen number (Kn) can be used to study the possibility of thermalization and applicability of hydrodynamics in a medium. Low values of Kn (Kn $\ll 1$) indicate systems with low gradients of hydrodynamic quantities, and thus the system is close to equilibrium (high degree of thermalization) [25]. A similar conclusion is also obtained in Ref. [26], where the applicability of fluid dynamics is strictly valid for cases of Kn ~ 1. In our previous study [27], we explored the possibility of fluid dynamics in the hadronic medium by studying Kn. We observed a considerably small value for Kn at high temperatures within the excluded volume hadron resonance gas

(EVHRG) formalism. In the current paper, we extend that study by explicitly deriving the valid equations for dissipative second-order (SO) hydrodynamics for a massive system and exploring the possibility of hydrodynamics in the hadronic phase by estimating the hadronic phase lifetime.

Short-lived resonances decay with a wide range of lifetimes, which allows them to be suitable probes for characterizing the properties of hadronic matter produced in heavy-ion collisions (see [28] and references therein) and also to estimate the hadronic phase lifetime. The resonances produced at the chemical freeze-out boundary can decay before the kinetic freeze-out, and their decay products undergo hadronic re-scattering, leading to a decrease in the resonance yields reconstructed at the kinetic freeze-out boundary. At the same time, pseudoelastic interactions between hadrons can regenerate the resonances in the medium, which increases the yields. Various transport and statistical thermal model calculations show that re-scattering and regeneration processes significantly affect the final state resonance yields [6,19,29–33]. These effects make them perfect probes to study the hadronic phase lifetime, as explored in Refs. [28,34]. In this paper, we follow an alternate approach and use Kn to govern the cooling of a hadronic medium from T_c using a viscous second-order (0+1D) hydrodynamic model to obtain the hadronic phase lifetime. We introduce a model for the evolution of resonance particle yields during the hadronic phase. The model is used within the ambit of hydrodynamic evolution to obtain the multiplicity and transverse momentum (p_T) dependent final yields, which are then compared with experimental data.

The paper is organized as follows. Section 2 details the equations derived for hydrodynamic calculations and the considerations that have been used to estimate the hadronic phase lifetime. Further, in Section 3, the formalism to obtain resonance yields at freeze out within a kinetic approach is detailed. In Section 4, we present the results along with discussions. Section 5 summarizes the study.

2. Expanding Hadronic Phase

LQCD calculations predict the existence of a deconfinement transition from hadronic to partonic constituents for energy densities greater than 1 GeV fm^{-3} [35]. At zero baryochemical potential (μ_B), this deconfinement transition is predicted again by LQCD to be of crossover in nature [36] at $T_c \simeq 155$ MeV [37–39]. The hadronic phase, thus predicted to be produced at the end of the QGP phase as a result of confinement, is further considered to expand and cool down. A sophisticated interplay of hadronic interactions, such as elastic and inelastic scattering, resonance production, decay, and other dynamical phenomena characterize the expanding hadronic phase. To precisely interpret the experimental data and deduce the properties of the QGP and the nature of the QCD phase transition, a thorough understanding of this complex phase is essential. It can provide unique insights into the fundamental properties of matter under extreme conditions, emphasizing the necessity for modeling this dynamic phase. In this Section, we explore the initial hadronization at chemical freeze-out and employ hydrodynamics to study the evolution of the hadronic medium and its cooling rate under various scenarios.

2.1. Statistical Hadronization

The hadronization of the QCD matter is crucial to exploring QCD thermodynamics, and this transformation is effectively captured through the use of statistical thermal models, such as the ideal HRG model. Within the HRG model, the partition function for the ith hadron in the grand canonical ensemble is given by [40];

$$\ln Z_i^{\mathrm{id}} = \pm \frac{V g_i}{2\pi^2} \int_0^\infty p^2 dp \ln\{1 \pm \exp[-(E_i - \mu_i)/T]\}, \quad (1)$$

where g_i, $E_i = \sqrt{p^2 + m_i^2}$ (with p, the momentum of a particle), and μ_i are the degeneracy, energy, and chemical potential of the ith hadron, respectively. V and T define the volume and the temperature of the system, respectively. μ_i is given by

$$\mu_i = B_i\mu_B + S_i\mu_S + Q_i\mu_Q, \tag{2}$$

where B_i, S_i, and Q_i are the baryon number, strangeness, and electric charge of the ith hadron. Here, μ_B, μ_S, μ_Q are the baryon, strange, and charge chemical potentials, respectively.

Knowing the partition function, one can calculate the pressure P_i, energy density ε_i, number density n_i, and entropy density s_i as follows:

$$P_i^{\mathrm{id}}(T,\mu_i) = \pm\frac{Tg_i}{2\pi^2}\int_0^\infty p^2dp\ln\{1\pm\exp[-(E_i-\mu_i)/T]\}, \tag{3}$$

$$\varepsilon_i^{\mathrm{id}}(T,\mu_i) = \frac{g_i}{2\pi^2}\int_0^\infty \frac{E_i\,p^2dp}{\exp[(E_i-\mu_i)/T]\pm 1}, \tag{4}$$

$$n_i^{\mathrm{id}}(T,\mu_i) = \frac{g_i}{2\pi^2}\int_0^\infty \frac{p^2dp}{\exp[(E_i-\mu_i)/T]\pm 1}, \tag{5}$$

$$s_i^{\mathrm{id}}(T,\mu_i) = \pm\frac{g_i}{2\pi^2}\int_0^\infty p^2dp\Big[\ln\{1\pm\exp[-(E_i-\mu_i)/T]\}\pm\frac{(E_i-\mu_i)/T}{\exp[(E_i-\mu_i)/T]\pm 1}\Big]. \tag{6}$$

The ideal HRG model can be further extended to the EVHRG model by the inclusion of van der Waals (vDW) repulsive interactions between hadrons by considering a fixed volume to be occupied by each hadron. If $v = 16\pi r_h^3/3$ is the volume occupied by each hadron where r_h is the hard-core radius, then the thermodynamic quantities in Equations (3)–(6) are given by [40,41]

$$P^{\mathrm{EV}}(T,\mu) = \kappa P^{\mathrm{id}}(T,\mu), \tag{7}$$

$$\varepsilon^{\mathrm{EV}}(T,\mu) = \frac{\kappa\varepsilon^{\mathrm{id}}(T,\mu)}{1+\kappa v n^{\mathrm{id}}(T,\mu)}, \tag{8}$$

$$n^{\mathrm{EV}}(T,\mu) = \frac{\kappa n^{\mathrm{id}}(T,\mu)}{1+\kappa v n^{\mathrm{id}}(T,\mu)}, \tag{9}$$

$$s^{\mathrm{EV}}(T,\mu) = \frac{\kappa s^{\mathrm{id}}(T,\mu)}{1+\kappa v n^{\mathrm{id}}(T,\mu)}, \tag{10}$$

where μ represents the chemical potential and κ is the excluded volume suppression factor given by

$$\kappa = \exp\left(\frac{vP^{\mathrm{EV}}}{T}\right). \tag{11}$$

These models have been used extensively to study particle production in nucleus-nucleus collisions. From these studies, it has been found that particle yields in the final state can be explained with considerable precision by these models at temperatures that are in agreement with the phase transition temperature predicted by LQCD [6,42,43]. In the following, we use the EVHRG model to determine the initial yields considering the chemical freeze-out temperature to be equal to $T_c = 156$ MeV as given by the Wuppertal–Budapest Collaboration [38,39].

2.2. Temperature Evolution of the Hadronic Medium

The hadronic medium produced at chemical freeze-out in nucleus-nucleus collisions is at a higher temperature and cools down with time. The temperature cooling can be studied by solving the first-order (FO) and SO fluid dynamical equations [44–46] derived within the framework of causal Müller–Israel–Stewart theory of dissipative fluid dynamics [47–49]. In the (0+1D) scaling solution, one obtains [44,46]:

$$\frac{\partial \varepsilon}{\partial \tau} = -\frac{\varepsilon + P}{\tau} + \frac{\phi}{\tau}. \tag{12}$$

The PF, FO, and SO theories are distinguished by ϕ, which defines the effect of viscous terms, as follows:

$$\phi = 0 \quad \text{(PF)}, \tag{13}$$

$$\phi = \frac{4\eta}{3\tau} \quad \text{(FO)}, \tag{14}$$

$$\frac{d\phi}{d\tau} = -\frac{\phi}{\tau_\phi} - \frac{\phi}{2}\left[\frac{1}{\tau} + \frac{1}{\beta_2} T \frac{d}{d\tau}\left(\frac{\beta_2}{T}\right)\right] + \frac{2}{3\beta_2 \tau} \quad \text{(SO)}, \tag{15}$$

where τ_ϕ is the relaxation time due to shear viscous component and $\beta_2 = \tau_\phi/(2\eta)$. In the SO theory, ϕ indicates the characteristics of the system by measuring the change in η through Equation (15). The solution of Equations (12) and (15) can be obtained numerically for a viscous system. The initial conditions for ϕ are calculated from the EVHRG model. Taking the AdS/CFT lower bound for $\eta/s = 1/(4\pi)$ [5], the value of ϕ at the time τ_c (τ at $T = T_c$) is found as $\phi_c = s_c/(3\pi\tau_c)$ with $s_c = s(\tau_c)$.

In Ref. [50], it has been shown that for a hadronic medium, the equilibration times of kaons and protons are larger than that of pions. Also to be noted is that pions, being the least massive of all hadrons, are abundantly produced at the chemical freeze-out, making pions the dominant component of the hadron gas phase. Thus, in the present paper, we approximate the dynamics or evolution of the hadronic phase to be determined by pions [50]. We consider two different cases in this regard: (a) massless pionic medium and (b) massive pionic medium.

The equations of system evolution for the massless case are already available in the literature [44,46] and are given by

$$\frac{dT}{d\tau} = -\frac{T}{3\tau} + \frac{\phi}{12aT^3\tau}, \tag{16}$$

$$\frac{d\phi}{d\tau} = -\sigma b T^3 \phi - \frac{1}{2}\left(\frac{1}{\tau} - 5\frac{1}{T}\frac{dT}{d\tau}\right) + \frac{8aT^4}{9\tau}, \tag{17}$$

where σ represents the interaction cross-section between pions and the constants are given by $a = \pi^2/30$ and $b = 3\zeta(3)/\pi^2$. Here $\zeta(\cdot)$ is the Euler–Riemann zeta function.

The cooling rate equations for the massive medium are derived in Section 2.3 just below.

2.3. Cooling Law for Massive Pionic Medium

We consider the case of a massive pion gas in the Boltzmann limit. It is a known result that the pressure is proportional to the particle number density times the temperature [41]:

$$P = a' n T, \tag{18}$$

where a' is the proportionality constant which is explicitly obtained using Equations (3) and (5). Now, using $P = c_s^2\varepsilon$, one obtains

$$\varepsilon = \frac{a'nT}{c_s^2}, \tag{19}$$

where the speed of sound squared, $c_s^2 = \partial P/\partial\varepsilon$, is calculated at each instant along the evolution considering a pionic medium.

On using Equations (18) and (19), Equation (12) is modified accordingly:

$$\frac{dT}{d\tau}\left(T\frac{\partial n}{\partial T} + n - \frac{nT}{c_s^2}\frac{\partial c_s^2}{\partial T}\right) = -\frac{nT}{\tau}(c_s^2+1) + \frac{\phi c_s^2}{a'\tau}, \tag{20}$$

where $\partial n/\partial T$ can be obtained using Equation (5):

$$\frac{\partial n}{\partial T} = \frac{\varepsilon}{T^2} = \frac{a'n}{c_s^2 T}. \tag{21}$$

Thus, Equation (20) modifies to

$$\frac{dT}{d\tau}\left(T\frac{a'n}{c_s^2 T} + n - \frac{nT}{c_s^2}\frac{\partial c_s^2}{\partial T}\right) = -\frac{nT}{\tau}(c_s^2+1) + \frac{\phi c_s^2}{a'\tau}, \tag{22}$$

which gives the temperature evolution for a massive viscous medium,

$$\frac{dT}{d\tau} = -\frac{c_s^2 T}{\tau}\left(\frac{c_s^2+1}{c_s^2 + a' - T\frac{\partial c_s^2}{\partial T}}\right) + \frac{\phi c_s^4}{a'n\tau\left(c_s^2 + a' - T\frac{\partial c_s^2}{\partial T}\right)}. \tag{23}$$

In the case of a massive PF ($\phi = 0$), this equation reduces to

$$\frac{dT}{d\tau} = -\frac{c_s^2 T}{\tau}\left(\frac{c_s^2+1}{c_s^2 + a' - T\frac{\partial c_s^2}{\partial T}}\right). \tag{24}$$

It has to be noted here that on replacing $a' = 1$, $c_s^2 = 1/3$, and $P = aT^4$, Equation (23) reduces to Equation (16), which is the temperature cooling rate at the massless limit.

The effect of viscosity in Equation (23) is determined by solving Equation (15), which can be solved in the Boltzmann limit by making use of the results obtained in Refs. [47,49]. β_2 is generally defined as

$$\beta_2 = \frac{1}{2\bar{\eta}^2 P}\left(1 + \frac{6\bar{\eta}}{\beta}\right), \tag{25}$$

where $\beta = m/T$ and $\bar{\eta} = (\varepsilon + P)/(nm) = (c_s^2+1)a'T/m$ with m being the rest mass of the particle, so that

$$\beta_2 = \frac{1}{2}\left[\left(\frac{(c_s^2+1)a'T}{m}\right)^2 a'nT\right]^{-1}\left(1 + \frac{6(c_s^2+1)a'T^2}{m^2}\right), \tag{26}$$

which gives,

$$\beta_2 = \frac{1}{2}\frac{m^2 + 6(c_s^2+1)a'T^2}{(c_s^2+1)^2(a'T)^3 n}. \tag{27}$$

From Equation (27),

$$\frac{\beta_2}{T} = \frac{1}{2a'^2 n(c_s^2+1)}\left(\frac{m^2}{T^4(c_s^2+1)a'} + \frac{6}{T^2}\right). \tag{28}$$

Using chain rule to solve Equation (15)), one finds

$$\frac{d}{d\tau}\left(\frac{\beta_2}{T}\right) = \frac{d}{dT}\left(\frac{\beta_2}{T}\right)\frac{dT}{d\tau}, \tag{29}$$

where $dT/d\tau$ is given by Equation (22). From Equation (28),

$$\frac{d}{dT}\left(\frac{\beta_2}{T}\right) = \frac{1}{2a'^2 n(c_s^2+1)}\left(-\frac{4m^2}{T^5(c_s^2+1)a'} - \frac{12}{T^3}\right) + \left(\frac{m^2}{T^4(c_s^2+1)a'} + \frac{6}{T^2}\right) \times \left(-\frac{1}{2a'^2 n^2(c_s^2+1)}\frac{\partial n}{\partial T}\right). \tag{30}$$

Then, using Equation (21), one obtains

$$\frac{d}{dT}\left(\frac{\beta_2}{T}\right) = \frac{1}{2a'^2 n(c_s^2+1)}\left(-\frac{4m^2}{T^5(c_s^2+1)a'} - \frac{12}{T^3}\right) + \frac{1}{2a' n c_s^2(c_s^2+1)}\left(-\frac{m^2}{T^5(c_s^2+1)a'} - \frac{6}{T^3}\right), \tag{31}$$

which further reduces to

$$\frac{d}{dT}\left(\frac{\beta_2}{T}\right) = -\frac{1}{2a' n(c_s^2+1)T^3}\left[\frac{12}{a'} + \frac{6}{c_s^2} + \frac{m^2}{T^2(c_s^2+1)a'}\left(\frac{4}{a'} + \frac{1}{c_s^2}\right)\right]. \tag{32}$$

Using Equations (27), (29), and (32) in Equation (15) gives

$$\frac{d\phi}{d\tau} = -\frac{\phi}{\tau_\phi} - \frac{\phi}{2}\left\{\frac{1}{\tau} - \frac{T(c_s^2+1)a'^2}{m^2+6(c_s^2+1)a'T^2}\left[\frac{12}{a'} + \frac{6}{c_s^2} + \frac{m^2}{T^2(c_s^2+1)a'}\left(\frac{4}{a'} + \frac{1}{c_s^2}\right)\right]\frac{dT}{d\tau}\right\} + \frac{4}{3\tau}\frac{T^3(c_s^2+1)^2 a'^3 n}{m^2+6(c_s^2+1)a'T^2}. \tag{33}$$

The only unknown quantity in Equation (33) is τ_ϕ. The particle-dependent relaxation time for a hadron gas can be obtained using the Boltzmann transport equation (BTE) [27,51,52]. For a scattering of ith and jth particles, $i(p_i) + j(p_j) \to i(p_k) + j(p_l)$, the energy-dependent relaxation time is given by

$${\tau_\phi}^{-1}(E_i) = \sum_{jkl}\int \frac{d^3p_j d^3p_k d^3p_l}{512\pi^9} W(i, j \to k, l) f_j^0, \tag{34}$$

where $W(i, j \to k, l)$ is the transition rate and f_j^0 is the distribution function. In the center-of-mass frame, Equation (34) reduces to

$${\tau_\phi}^{-1}(E_i) = \sum_j \int \frac{d^3p_j}{8\pi^3}\sigma_{ij} v_{ij} f_j^0, \tag{35}$$

where σ_{ij} is the interaction cross-section and v_{ij} is the relative velocity. Equation (35) can be averaged over f_i^0 to obtain the averaged relaxation time $\tilde{\tau}_{i\phi}$ for particle i:

$$\tilde{\tau}_{i\phi}^{-1} = \frac{\int \frac{d^3p_i}{8\pi^3}\tau^{-1}(E_i)f_i^0}{\int \frac{d^3p_i}{8\pi^3}f_i^0} = \sum_j \frac{\int \frac{d^3p_i}{8\pi^3}\frac{d^3p_j}{8\pi^3}\sigma_{ij}v_{ij}f_i^0 f_j^0}{\int \frac{d^3p_i}{8\pi^3}f_i^0} = \sum_j n_j\langle\sigma_{ij}v_{ij}\rangle. \quad (36)$$

The thermal averaged cross-section times relative velocity is given by [27,51,52];

$$\langle\sigma_{ij}v_{ij}\rangle = \frac{\sigma\int p_i p_j E_i\, dE_i\, E_j\, dE_j\, d\cos\theta\, f_i^0 f_j^0 \times \frac{\sqrt{(E_i\,E_j - p_i p_j\cos\theta)^2 - (m_i m_j)^2}}{E_i\,E_j - p_i p_j\cos\theta}}{\int p_i p_j E_i\, dE_i\, E_j\, dE_j\, d\cos\theta\, f_i^0 f_j^0}, \quad m_i, m_j \to \infty, \quad (37)$$

where E_i and E_j are particles' energies and θ is the angle between the particles' momenta p_i and p_j. The integration over $\cos\theta$ is taken from -1 to $+1$. f_i^0 in Equation (37) is given by

$$f_i^0 = \exp\left(-\frac{E_i - \mu_B}{T}\right), \quad (38)$$

where μ_B is set to zero in our calculations.

Equation (36) is used to find the pion relaxation times at different temperatures and the values obtained are fitted by an exponent $\tau_\phi = A\exp(-\lambda T)$, as shown in Figure 1, to obtain an approximate dependence on temperature. This fit function is further used in Equation (33).

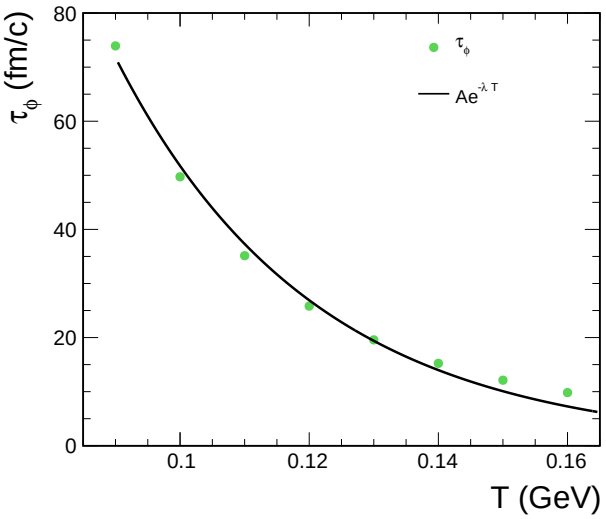


Figure 1. Relaxation time τ_ϕ of a massive pion gas as a function of temperature T. The fit parameters obtained are $A = 1362.73 \pm 212.198$ fm/c and $\lambda = 32.7087 \pm 1.5375$ GeV^{-1}.

Equations (24) and (33) describe the cooling rate for massive pion gas. In our calculations, we assume $m_\pi = 0.139$ GeV.

2.4. Transverse Correction to the Cooling Law

The effect of transverse expansion can be included in the (0+1D) scaling solution for the partonic state by considering that cooling is defined by the transverse expanded time $\tau_{tr} > \tau$, i.e., $T_{tr}(\tau) < T(\tau)$ [7,8,53]. This also implies that the temperature cooling begins at a lower temperature $T_{tr}(\tau_0) < T_0(\tau_0)$, with τ_0 being the initial thermalization time. Such a consideration makes cooling faster due to the effect of transverse expansion. Thus, due to

the transverse expansion from the initial phase of collision, the system achieves chemical freeze-out temperature, T_c, earlier than in a simplified (0+1D) expansion.

Let us define chemical freeze-out time as $\tau_{\rm QGP}$. In the case of ideal expansion without transverse cooling, one may roughly assume that the QGP fireball lifetime $\tau^{\rm id}_{\rm QGP} = R_T$ [54], where R_T is the transverse radius obtained from the MC Glauber model [55]. Taking a similar approach but with the transverse expansion, one may assume the hadronization to take place when $\tau_{\rm tr} = R_T$. Now, defining $\tau_{\rm tr} \cong \tau^{\rm tr}_{\rm QGP} + \frac{R_T}{c_s}\frac{\sqrt{2}-1}{\sqrt{2}}$, $\tau^{\rm tr}_{\rm QGP}$ can be straightforwardly determined [53]. $\tau^{\rm tr}_{\rm QGP}$ is further used as the hadronization time τ_c defined earlier as the initial time τ_0 for the hydrodynamical evolution of the hadronic phase.

Figure 2 (left) compares the temperature evolution of the massive and massless cases of PF and SO hydrodynamic models along with the FO massless case. One can see that viscous terms make cooling slower. The SO theory leads to a much faster cooling rate than the FO theory. The effect of particle mass makes cooling slower, as observed in the PF limit. Figure 2 (right) shows the impact of particle mass on the viscous component, which slows down cooling by generating more heat. In the case of massless particles, viscosity is higher and decays slowly as compared to the massive case. Thus, slowing down of the cooling for massive cases is opposed by the lower viscosity in the SO hydrodynamics as compared to the massless case. An interplay of these effects can be seen in the massive SO theory results in Figure 2 (left), which is close enough to the massless condition albeit slightly slower. In the following, we consider only the SO model cooling scenario, because the FO theory solution is acausal and leads to unstable results [44].

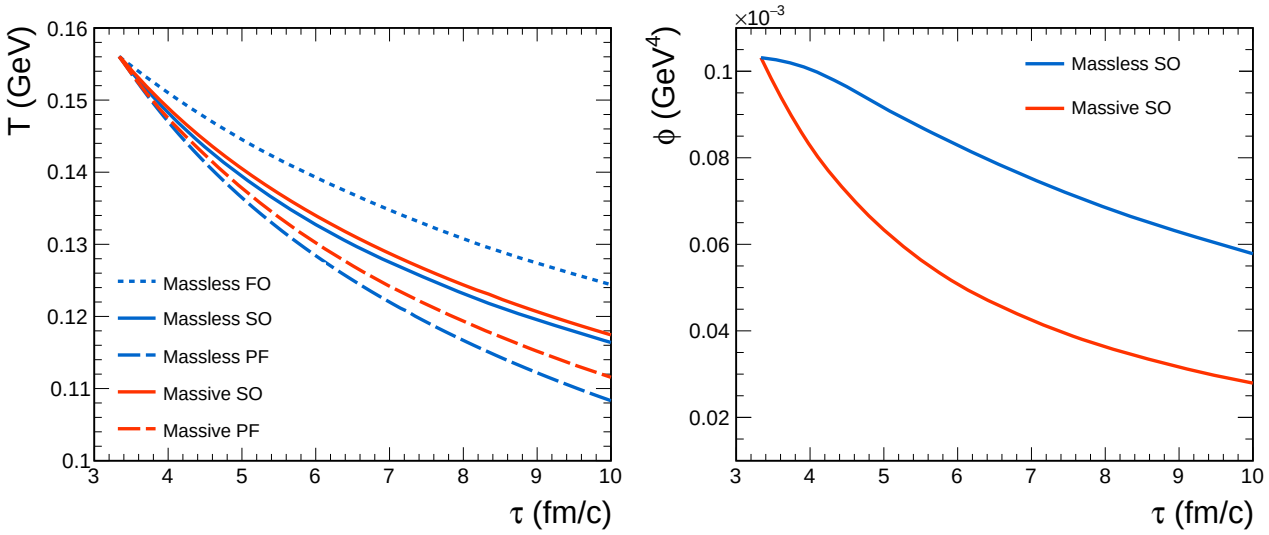


Figure 2. (**Left**): temperature evolution as a function of proper time for both massive and massless constituent pions as calculated for the first-order (FO), and second-order (SO) hydrodynamical theories and the perfect liquid (PF) limit. The initial temperature is taken as $T_c = 0.156$ GeV to start the cooling law from the chemical freeze-out [38,39]. (**Right**): comparison of the viscous component as a function of proper time for massive and massless SO hydrodynamics. See text for details.

The validity of hydrodynamics is governed by Kn. Kn describes the probability of collisions between the particles in the system. Kn $\ll 1$ indicates that the system size is larger than the mean free path, indicating thermalization. Therefore, it becomes feasible to study the medium evolution under hydrodynamics.

Kn is defined as

$$\text{Kn} = L/D, \tag{39}$$

where $L = 1/(\sqrt{2}n\sigma)$ is the mean free path of the system, n and $\sigma = 4\pi r_h^2$ are the number density and the interaction cross-section between the particles of the medium, respectively.

$D = 2R$ is the characteristic system size, where R denotes the system transverse radius. Hydrodynamic evolution ends and the equilibrium is considered to break down at the moment when the mean free path becomes greater than the system size, i.e., at Kn > 1 [26]. The time-dependent transverse radius used in Equation (39) can be obtained following the method given in Ref. [53], where the effective radius at a time $\tau > \tau_i$ is given by

$$R \cong R_i \left(1 + \frac{1}{6}\sqrt{\frac{1}{\tau_i}}\frac{(\tau - \tau_i)^{3/2}}{R_i}\right), \tag{40}$$

where τ_i is the proper time at the previous instant.

3. Kinetic Formation Model for Resonance Particles

At the end of the QGP phase, the deconfined quarks and gluons are combined to form hadrons, entering the hadronic phase. As a result of confinement, physical observables such as particle spectra, flow, fluctuations and correlations, etc., in QCD are required to be defined in terms of hadrons. The dynamics of interactions within the hadronic phase can affect these observables. These interactions involve both elastic scatterings, which change the momentum distribution without altering the particle composition, and inelastic processes, such as resonance formation and decay, that modify the chemical composition of the hadronic matter. This transport and evolution of hadrons in the hadronic phase strongly influence the final particle yields.

Several resonance particles are produced in the final state of proton–proton and heavy-ion collisions with lifetimes varying from 1.1 fm/c (for $f_2(1270)$) to 46.3 fm/c (for $\phi(1020)$), with c denoting the speed of light. Such a wide range in the lifetimes provides an exceptional opportunity to use them as probes to study the system formed in relativistic nuclear collisions [28,56–59]. The dynamics of these resonances within the hadronic phase significantly affect the yields and momentum distributions of the stable final state particles like pions, kaons and protons. Long-lived particles like η (with the lifetime $\tau_l \sim 10^{-19}$ s) and η' ($\tau_l \sim 10^{-21}$ s) mesons can also affect the final state pion yield obtained at detectors through their decay channels. In the subsequent calculations, we used three different resonance particles—namely, $\rho(770)^0$, $K^*(892)^0$, and $\phi(1020)$. Out of these, the $K^*(892)^0$ meson occupies a sweet spot, with a lifetime of 4.16 fm/c, making it a suitable probe to study the hadronic phase and hadronic phase lifetime, as performed in [28]. If the resonance decays within the hadronic phase, then the decay products are subject to interactions before kinetic freeze out, which alters their momentum and prevents their reconstruction (re-scattering) ($\rho(770)^0 \to \pi^+\pi^-$, $K^*(892)^0 \to \pi K$, $\phi(1020) \to K^+K^-$). Similarly, hadrons in the medium can interact together to form resonances that may live up to the kinetic freeze-out allowing a successful reconstruction (regeneration) ($\pi^+\pi^- \to \rho(770)^0$, $\pi K \to K^*(892)^0$, $K^+K^- \to \phi(1020)$). To obtain an experimental estimate of the hadronic phase lifetime, a natural decay formalism of $K^*(890)^0$ mesons is considered as given by [28,34]

$$\left[\frac{K^*}{K}\right]_{\text{kin}} = \left[\frac{K^*}{K}\right]_{\text{chem}} \exp\left(\frac{\tau_H}{\tau_l}\right), \tag{41}$$

where τ_H is the hadronic phase lifetime and the subscripts "kin" and "chem" denote the kinetic and chemical freeze-out boundaries, respectively. This formalism considers only rescattering due to decay and does not take into consideration the regeneration effects described above. Thus, it is imperative to include both of these effects in the calculations while studying the final resonance yields.

In this respect, we use a modified version of the kinetic formation model used to explain the yield of J/ψ meson in the final state [60,61]. This model was subsequently

modified to include transverse momentum dependence of the decay and regeneration cross-sections [7,8]. According to this model, the final state yield of resonance particles ($A \rightleftharpoons BC$) is given by

$$N_f^A(\tau_f, p_T) = \epsilon(\tau_f, p_T)\lambda_D(\tau_f, p_T)\left[N_i^A(\tau_c, p_T) + N^B(p_T)N^C(p_T) \times \int_{\tau_c}^{\tau_f} \Gamma_F(p_T)[V(\tau)\epsilon(\tau, p_T)\lambda_D(\tau, p_T)]^{-1} d\tau\right], \quad (42)$$

where $\lambda_D(\tau, p_T)$ and $\epsilon(\tau, p_T)$ give the contribution due to natural decay and co-moving hadrons, respectively, to re-scattering at time τ while $\Gamma_F(p_T)$ gives the effect of regeneration. τ_f denotes the kinetic freeze-out time. The quantities $N_i^A(\tau_c, p_T)$, $N^B(p_T)$ and $N^C(p_T)$ represent the p_T-dependent numbers of resonance particles and their decay products at chemical freeze-out determined through the EVHRG model. $N^B(p_T)$ and $N^C(p_T)$ are estimated such that their combination can produce a resonance particle at a given p_T.

The $V(\tau)$ in Equation (42) denotes the time-dependent volume of the evolving system. It is obtained considering the isentropic evolution of the hadronic phase. Based on the yields of weakly bound nuclei in the final states, it was suggested that any further evolution of the fireball after T_c has to be close to isentropic [6,62]. Further, in Ref. [54], it was quantitatively shown that for viscous hydrodynamic evolution, entropy production is minimal for the extended period when freeze-out is introduced. Thus, the volume profile $V(\tau, b)$ of the medium is obtained as follows:

$$V(\tau, b) = \frac{V_c(\tau_c, b)s_c(\tau_c)}{s(\tau)}, \quad (43)$$

where $V_c(\tau_c, b) = \tau_{\rm tr} A_T(b)$ is the initial volume at τ_0 with b the impact parameter and A_T being the transverse overlap area obtained from the MC Glauber model [55].

3.1. Regeneration

Regeneration of resonance particles in the hadronic phase is modeled in Equation (42) through $\Gamma_F(p_T)$, which is given by

$$\Gamma_F(p_T) = \langle \sigma_{\rm reg}^A(p_T) v_{\rm rel} \rangle_{B,C}\,, \quad (44)$$

where the averaging $\langle \cdots \rangle_{B,C}$ is taken over the B and C particles as is prescribed in Equation (37), $\sigma_{\rm reg}(p_T)$ is the regeneration cross-section, and $v_{\rm rel}$ is the relative velocity between the particles. For $\rho(770)^0$ and $K^*(892)^0$ mesons, the temperature-dependent regeneration cross-sections ($\sigma_{\rm reg}(T)$) are given by [63]

$$\sigma_{\rm reg}^{\rho}(T) = 54.1\left(\frac{T/T_c - 0.42}{0.18}\right)^{3.3} \exp\left[3.3\left(1 - \frac{T/T_c - 0.42}{0.18}\right)\right] + 5.32\left(\frac{T/T_c - 0.42}{0.5}\right)^{84} \exp\left[84\left(1 - \frac{T/T_c - 0.42}{0.5}\right)\right], \quad (45)$$

$$\sigma_{\rm reg}^{K^*}(T) = 42.2\left(\frac{T/T_c - 0.5}{0.115}\right)^{1.83} \exp\left[1.83\left(1 - \frac{T/T_c - 0.5}{0.115}\right)\right] + 4.95\left(\frac{T/T_c - 0.5}{0.407}\right)^{50} \exp\left[50\left(1 - \frac{T/T_c - 0.5}{0.407}\right)\right], \quad (46)$$

where the critical temperature was taken to be $T_c = 0.175$ GeV. In the absence of such temperature-dependent parameterizations for $\phi(1020)$ mesons, we used the vacuum cross-section of 8.05 mb [64] at all temperatures, i.e., $\sigma_{\rm reg}^{\phi}(T) = 8.05$ mb.

The temperature experienced by the resonance particle can differ from the medium temperature. Thus, we use the relativistic Doppler shift due to the relative velocity v_r of resonance as compared to the medium to obtain the effective temperature felt by the resonance particle. The effective temperature is given by [7,65,66]

$$T_{\rm eff}(\tau, p_T) = T(\tau)\ \frac{\sqrt{1-|v_r|^2}}{2|v_r|}\ \ln\left(\frac{1+|v_r|}{1-|v_r|}\right). \tag{47}$$

To calculate v_r, we used the medium velocity $v_m = 0.5c$ comparable to the expansion velocity obtained from blastwave fits to data [67] and the resonance velocity $v_A = p_T/E_T$ with the transverse energy $E_T = \sqrt{p_T^2 + m_A^2}$, where m_A is the mass of the particle A. Thus, the p_T-dependent regeneration cross-sections $\sigma^A_{\rm reg}(p_T)$ are obtained from the temperature-dependent cross-sections $\sigma^A_{\rm reg}(T)$ by using $T = T_{\rm eff}(\tau, p_T)$.

3.2. Decay

The re-scattering effect introduced in Equation (42) was modeled to include two different effects. Resonance particles produced at chemical freeze-out can undergo natural decay ($A \to BC$). They might also decay as a result of interaction with another particle (X) within the medium (co-moving hadron): $AX \to BCX$. We consider that the resonance particle is re-scattered in both cases. The contribution due to natural decay is given by

$$\lambda_D(\tau, p_T) = \exp\left(-\frac{\tau - \tau_c}{\tau_l(p_T)}\right), \tag{48}$$

where $\tau_l(p_T) = \tau_{\rm res}\gamma(p_T)$ is a product of the vacuum lifetime $\tau_{\rm res}$ of the resonance particle and the p_T-dependent Lorentz factor, the latter, in our calculations considered to read $\gamma(p_T) = \sqrt{1 + (p_T/mc)^2}$ [28]. The effect of co-moving hadrons is modeled based on the kinetic model [60,61]:

$$\epsilon(\tau, p_T) = \exp\left[-\int_{\tau_c}^{\tau} \Gamma_D(p_T) N_{\rm co}[V(\tau)]^{-1} d\tau\right], \tag{49}$$

where $N_{\rm co}$ represents the total number of the co-moving hadrons and $\Gamma_D(p_T)$ is the decay rate of the resonances averaged over the co-moving hadron momentum distribution and is given by

$$\Gamma_D(p_T) = \langle \sigma^A_{\rm co}(p_T) v_{\rm rel} \rangle_{A,{\rm co}}, \tag{50}$$

where $\sigma^A_{\rm co}(p_T)$ is the p_T-dependent decay cross-section. This decay cross-section is obtained by using detailed balance from the regeneration cross-section $\sigma^A_{\rm reg}(p_T)$ [7,61]. $\langle \sigma v \rangle$ term in Equation (50) is obtained for particle A and the co-moving hadron using Equation (37).

4. Results and Discussion

The hadronic medium considered in this paper, consists of all hadrons and resonances with masses up to 2.25 GeV given in the *Review of Particle Physics* book [68]. Since the properties of the medium depend on the parameter r_h, it has to be chosen appropriately. The repulsive interactions being mediated by ω meson and the range of interaction being inversely proportional to the mass of the mediator, we have chosen the hard-core radius, $r_h = 0.25$ fm to incorporate repulsive interactions. This radius is chosen to be uniform for all hadrons.

The Knudsen number is an essential parameter as it indicates the applicability of hydrodynamics in the medium. As discussed in Section 2, we used this parameter to obtain the endpoint τ_f for hydrodynamics. Finding τ_f allows us to estimate the hadronic phase

lifetime τ_H just by calculating the difference between the initial (τ_c) and final (τ_f) time. In Figure 3, we depict the hadronic phase lifetime obtained in our calculations for both the massive and massless SO hydrodynamics and compare it with the 5.02 TeV Pb–Pb collision results from the LHC [28]. The massive SO theory predicting a slightly slower cooling rate than the massless case (as seen in Figure 2), gives a higher lifetime. A reasonable agreement is observed between our calculations and the experimental results in both cases.

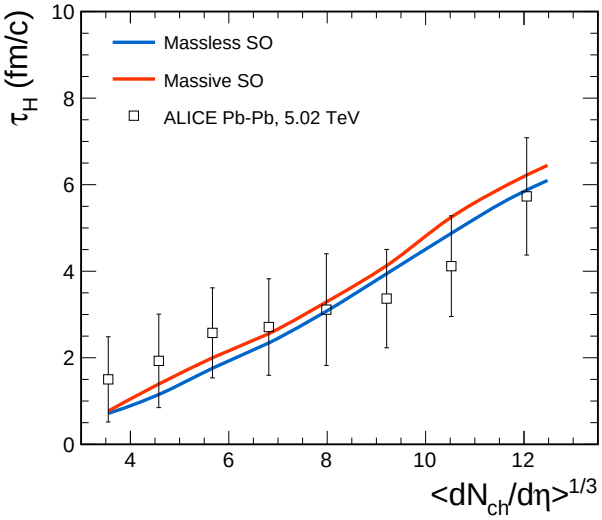


Figure 3. Hadronic phase lifetime obtained from the calculations are compared with the results obtained from Pb–Pb collisions at the nucleon–nucleon center-of-mass energy $\sqrt{s_{\rm NN}}$ = 5.02 TeV by the ALICE experiment [28].

Further, we investigate the p_T-dependent natural decay, co-moving hadron-induced decay, and regeneration of the resonance particles within the hadronic phase as given by Equation (48), (50), and (44), respectively. The results for the (0–5)% centrality (most central) Pb–Pb collisions at the nucleon-nucleon center-of-mass energy $\sqrt{s_{NN}} = 5.02$ TeV with these parameters are presented in Figure 4. In Figure 4 (left), the natural decay rate is analyzed as a function of momentum for different resonance particles. At high p_T, the time dilation causes λ_D to increase and approach unity. The impact of particle lifetime on the survival probability is evident, as the $\phi(1020)$ meson with $\tau_{\rm res} = 46.3$ fm/c is relatively unaffected beyond $p_T = 2$ GeV/c. In contrast, the yields of $\rho(770)^0$ mesons, which have $\tau_{\rm res} = 1.3$ fm/c, are reduced over an extended p_T range. The middle and right panels of Figure 4 displays the p_T-dependent interaction rates for co-mover-induced decay and regeneration, respectively. It is observed that decay and regeneration are more likely at low p_T for all the considered resonances. These probabilities decrease further and saturate towards high p_T, which can be attributed to the initial particle production at these p_T intervals. It is more probable for particles at low p_T to move together, favoring the interaction, compared to particles with high p_T. In the following discussions, "ND", "CMD", and "R" mark natural decay, co-moving hadron-induced decay, and regeneration effects, respectively. The individual effects of the regeneration, decay due to co-moving hadrons, and natural decay are explicitly studied.

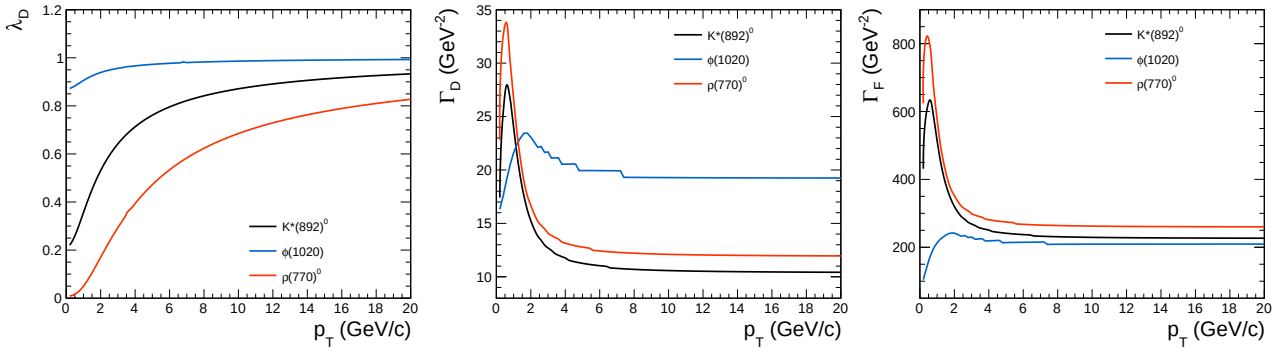


Figure 4. The natural decay parameter λ_D (**left**), dissociation reactivity Γ_D (**middle**), and regeneration reactivity Γ_F (**right**) explored as a function of transverse momentum (p_T) for $K^*(892)^0$, $\phi(1020)$, and $\rho(775)^0$.

The combined effects of these mechanisms on the resonance yields are further studied and shown in Figure 5 as a function of p_T. The particle ratios are shown only for the "ND+CMD+R" and "ND+CMD" cases, as the "ND+R" case is nearly identical to the "ND+CMD+R" scenario. In all the three particle ratios considered, a qualitative agreement is obtained for $p_T < 3$ GeV for the "ND+CMD+R" case beyond which the particle ratios are overestimated. However, a complete description of the full p_T range is not expected due to the limitations of hydrodynamic calculations and its ability to account for high p_T particles. In the absence of regeneration effects, these ratios tend to be much lower towards higher p_T. This indicates that our model overestimates regeneration effects towards the high p_T region. Such an overestimation is mainly due to the effect of the initially obtained p_T-dependent daughter particle numbers, which was seen to overshadow the initial resonance particle production. Thus, the final particle numbers obtained at high p_T tend to increase rapidly. A more complete description would be needed to account for these effects and obtain the saturating out of particle ratios to high p_T seen experimentally.

Figure 6 depicts the final state particle ratios of resonances to stable particles obtained in heavy-ion collisions. Figure 6 compares the values obtained in our calculations for massive SO theory to the experimentally obtained $K^*(892)^0/K$, $\phi(1020)/K$ and $\rho(775)^0/\pi$ ratios [28,69–72]. The massless SO case is not shown here as it does not account for a realistic scenario. Also, there is a small change in hadronic phase lifetime as compared to the massive case shown in Figure 3. A considerable agreement with experimental values is obtained for $K^*(892)^0/K$ and $\phi(1020)/K$ estimates, even though $\sigma^{\phi}_{\mathrm{reg}}(T)$ is approximated to be constant. At the same time, $\rho(775)^0/\pi$ values are underestimated, especially at the high multiplicity regions. The natural decay component plays a significant part in determining the trends obtained for $K^*(892)^0/K$ and $\rho(775)^0/\pi$ estimates due to their sufficiently small lifetimes. For $\phi(1020)/K$, with λ_D being large, as seen in Figure 4, there is quite a little change due to natural decay. It can also be seen that both co-moving hadron-induced decay and regeneration effects play significant roles at high multiplicity bins, while their impact on low multiplicities is marginal. Our study suggests that these effects must be considered while using resonances as a probe to study the hadronic phase produced in relativistic nuclear collisions.

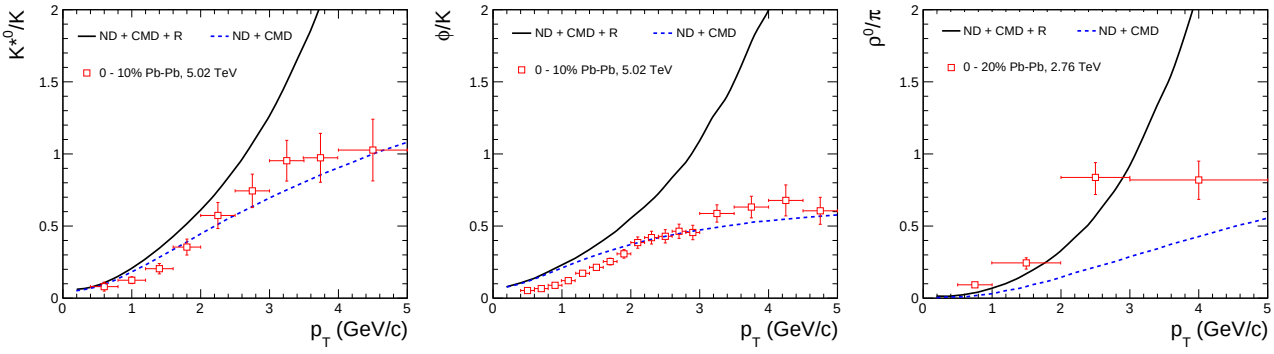


Figure 5. Transverse-momentum (p_T) dependence of $K^*(892)^0/K$ (**left**), $\phi(1020)/K$ (**middle**), and $\rho(775)^0/\pi$ (**right**) ratios compared to the results from the ALICE experiment [28,70]. See text for details.

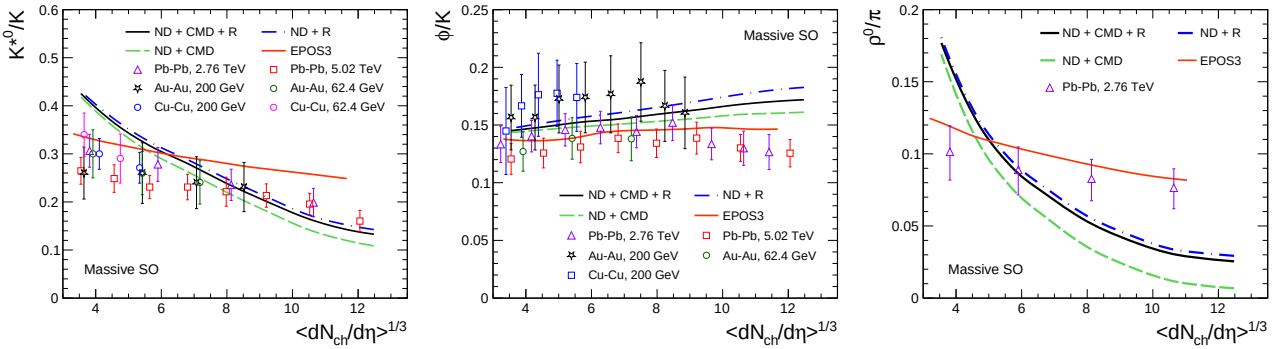


Figure 6. The estimated ratios of $K^*(892)^0/K$ (**left**), $\phi(1020)/K$ (**middle**), and $\rho(775)^0/\pi$ (**right**) obtained using the calculations here compared to the data [28,69–72] by the ALICE and RHIC experiments obtained with different colliding species. The results [28,70] from the EPOS3 model with UrQMD hadronic evolution are also shown for comparison. See text for details.

5. Summary

In this study, a hydrodynamic description is employed in the hadronic phase motivated through the dimensionless parameter, the Knudsen number, which implies the applicability of hydrodynamics. We consider a case where the regime between chemical freezeout and kinetic freezeout is dominated by hadronic scatterings but still maintains the applicability of hydrodynamics. We have found that the lifetime obtained through a hydrodynamic description of the hadronic phase is comparable with the results obtained at the ALICE experiment at LHC. Further, it is observed that the hadronic phase lifetime increases with the system size, which is manifested here in terms of charged-particle pseudorapidity density $\langle dN_{\rm ch}/d\eta \rangle$. We have shown that in heavy-ion collisions, the hadronic phase lifetime varies between 0.5 fm to about 6 fm from ultra-peripheral to most-central collisions, respectively. We have also explored the yield modification of the resonance particles due to the natural decay and dissociation due to the co-moving hadrons during the hydrodynamic evolution of the hadronic phase. The regeneration of the resonances due to the combination of the required hadrons is also studied, and it is found that regeneration plays a crucial role besides dissociation mechanisms in obtaining the net yield of the resonance particles moving in the expanding system. The interplay between the decay and regeneration processes determines the final state yields of these particles. The obtained results are compared with corresponding experimental data. These results qualitatively explain the experimental results at (low) $p_T \leq 3$ GeV as expected, because at high p_T, the applicability of the hydrodynamics is questionable. Further, p_T-integrated

resonance particle ratios are obtained against charged particle multiplicity and compared with corresponding experimental results, showing considerable agreement.

Particle interactions in the hadronic phase significantly affect the final state particle yields [6]. These interactions can also affect particle correlations, leading to modifications to the corresponding values at the chemical freeze-out boundary [73]. Estimating the hadronic phase lifetime and decoupling the effects of these interactions is thus necessary to obtain precise information about the QCD fireball. The present study explored the applicability of hydrodynamics, considering only massive pions as a component of the thermalized fluid using 0+1D viscous Bjorken-like flow. However, other abundant hadrons must be included as a part of the fluid, along with an extended 3+1D viscous hydrodynamics, for a comprehensive study. Such a comprehensive study can be performed with proper treatment of partial chemical equilibrium along the evolution. Furthermore, the estimates obtained here can have uncertainties due to the interaction cross-sections chosen from EVHRG, as the interaction cross-sections are poorly known near the chemical freeze-out boundary. These may be addressed by a proper estimation of the hadronic interaction cross-sections.

Author Contributions: All authors contributed equally to the work. All authors have read and agreed to the published version of the manuscript.

Funding: Ronald Scaria acknowledges the Council of Scientific & Industrial Research (CSIR), Ministry of Science and Technology, the Government of India, for the research fellowship. Raghunath Sahoo and Captain R. Singh acknowledge the financial support under the Board of Research in Nuclear Sciences of the Department of Atomic Energy (DAE-BRNS), the Government of India, Project No. 58/14/29/2019-BRNS.

Data Availability Statement: The experimental data used are available in the references cited. The calculations can be obtained on a reasonable request to the corresponding author.

Acknowledgments: The authors acknowledge the Tier-3 computing facility in the experimental high-energy physics laboratory of IIT Indore, supported by the ALICE project.

Conflicts of Interest: The authors declare no conflicts of interest.

Abbreviations

The following abbreviations are used in this manuscript:

AdS	anti-de Sitter
ALICE	A Large Ion Collider Experiment
AMPT	A Multi-Phase Transport
BTE	Boltzmann transport equation
CFT	Conformal field theory
EPOS	Energy conserving quantum mechanical approach, based on Partons, parton ladders, strings, Off-shell remnants, and Saturation of parton ladders
EV	excluded volume
HRG	hadron resonance gas
FO	first-order
LHC	Large Hadron Collider
LQCD	Lattice QCD
MC	Monte Carlo
PCE	partial chemical equilibrium
PF	perfect fluid
QCD	quantum chromodynamics
QGP	quark–gluon plasma
RHIC	Relativistic Heavy-Ion Collider

SO	second-order
UrQMD	Ultra-relativistic Quantum Molecular Dynamics (model)
vdW	van der Waals
0+1D	temporal one-dimensional
3+1D	three-spatial and temporal dimensional

References

1. Arsene, I. et al. [BRAHMS Collaboration] Quark–gluon plasma and color glass condensate at RHIC? The perspective from the BRAHMS experiment. *Nucl. Phys. A* **2005**, *757*, 1–27. [CrossRef]
2. Back, B.B. et al. [PHOBOS Collaboration] The PHOBOS perspective on discoveries at RHIC. *Nucl. Phys. A* **2005**, *757*, 28–101. [CrossRef]
3. Adams, J. et al. [STAR Collaboration] Experimental and theoretical challenges in the search for the quark gluon plasma: The STAR Collaboration's critical assessment of the evidence from RHIC collision. *Nucl. Phys. A* **2005**, *757*, 102–183. [CrossRef]
4. Adcox, K. et al. [PHENIX Collaboration] Formation of dense partonic matter in relativistic nucleus-nucleus collisions at RHIC: Experimental evaluation by the PHENIX collaboration. *Nucl. Phys. A* **2005**, *757*, 184–283. [CrossRef]
5. Kovtun, P.; Son, D.T.; Starinets, A.O. Viscosity in strongly interacting quantum field theories from black hole physics. *Phys. Rev. Lett.* **2005**, *94*, 111601. [CrossRef]
6. Andronic, A.; Braun-Munzinger, P.; Redlich, K.; Stachel, J. Decoding the phase structure of QCD via particle production at high energy. *Nature* **2018**, *561*, 321–330. [CrossRef]
7. Singh, C.R.; Ganesh, S.; Mishra, M. Centrality and transverse momentum dependent suppression of $\Upsilon(1S)$ and $\Upsilon(2S)$ in p−Pb and Pb−Pb collisions at the CERN Large Hadron Collider. *Eur. Phys. J. C* **2019**, *79*, 147. [CrossRef]
8. Singh, C.R.; Deb, S.; Sahoo, R.; Alam, J. Charmonium suppression in ultra-relativistic proton–proton collisions at LHC energies: A hint for QGP in small systems. *Eur. Phys. J. C* **2022**, *82*, 542. [CrossRef]
9. Bebie, H.; Gerber, P.; Goity, J.L.; Leutwyler, H. The role of the entropy in an expanding hadronic gas. *Nucl. Phys. B* **1992**, *378*, 95–128. [CrossRef]
10. Becattini, F. Universality of thermal hadron production in pp, $p\bar{p}$ and e^+ e^- collisions. *arXiv* **1996**. [CrossRef]
11. Motornenko, A.; Vovchenko, V.; Greiner, C.; Stoecker, H. Kinetic freeze-out temperature from yields of short-lived resonances. *Phys. Rev. C* **2020**, *102*, 024909. [CrossRef]
12. Bernhard, J.E.; Moreland, J.S.; Bass, S.A. Bayesian estimation of the specific shear and bulk viscosity of quark–gluon plasma. *Nat. Phys.* **2019**, *15*, 1113–1117. [CrossRef]
13. Parkkila, J.E.; Onnerstad, A.; Taghavi, S.F.; Mordasini, C.; Bilandzic, A.; Virta, M.; Kim, D.J. New constraints for QCD matter from improved Bayesian parameter estimation in heavy-ion collisions at LHC. *Phys. Lett. B* **2022**, *835*, 137485. [CrossRef]
14. Bernhard, J.E.; Moreland, J.S.; Bass, S.A.; Liu, J.; Heinz, U. Applying Bayesian parameter estimation to relativistic heavy-ion collisions: Simultaneous characterization of the initial state and quark–gluon plasma medium. *Phys. Rev. C* **2016**, *94*, 024907. [CrossRef]
15. Parkkila, J.E.; Onnerstad, A.; Kim, D.J. Bayesian estimation of the specific shear and bulk viscosity of the quark–gluon plasma with additional flow harmonic observables. *Phys. Rev. C* **2021**, *104*, 054904. [CrossRef]
16. Petersen, H.; Steinheimer, J.; Burau, G.; Bleicher, M.; Stöcker, H. Fully integrated transport approach to heavy ion reactions with an intermediate hydrodynamic stage. *Phys. Rev. C* **2008**, *78*, 044901. [CrossRef]
17. Lin, Z.-W.; Ko, C.M.; Li, B.-A.; Zhang, B.; Pal, S. A Multiphase transport model for relativistic heavy ion collisions. *Phys. Rev. C* **2005**, *72*, 064901. [CrossRef]
18. Steinheimer, J.; Aichelin, J.; Bleicher, M.; Stöcker, H. Influence of the hadronic phase on observables in ultrarelativistic heavy ion collisions. *Phys. Rev. C* **2017**, *95*, 064902. [CrossRef]
19. Knospe, A.G.; Markert, C.; Werner, K.; Steinheimer, J.; Bleicher, M. Hadronic resonance production and interaction in partonic and hadronic matter in the EPOS3 model with and without the hadronic afterburner UrQMD. *Phys. Rev. C* **2016**, *93*, 014911. [CrossRef]
20. Song, H.; Bass, S.A.; Heinz, U. Viscous QCD matter in a hybrid hydrodynamic+Boltzmann approach. *Phys. Rev. C* **2011**, *83*, 024912. [CrossRef]
21. Demir, N.; Bass, S.A. Shear-viscosity to entropy-density ratio of a relativistic hadron gas. *Phys. Rev. Lett.* **2009**, *102*, 172302. [CrossRef] [PubMed]
22. Romatschke, P. Collective flow without hydrodynamics: Simulation results for relativistic ion collisions. *Eur. Phys. J. C* **2015**, *75*, 429. [CrossRef]
23. Berges, J.; Borsányi, S.; Wetterich, C. Prethermalization. *Phys. Rev. Lett.* **2004**, *93*, 142002. [CrossRef] [PubMed]
24. Romatschke, P. Relativistic fluid dynamics far from local equilibrium. *Phys. Rev. Lett.* **2018**, *120*, 012301. [CrossRef]

25. Romatschke, P.; Romatschke, U. *Relativistic Fluid Dynamics In and Out of Equilibrium (and Applications to Relativistic Nuclear Collisions)*; Cambridge University Press: Cambridge, UK, 2019. [CrossRef]
26. Gallmeister, K.; Niemi, H.; Greiner, C.; Rischke, D.H. Exploring the applicability of dissipative fluid dynamics to small systems by comparison to the Boltzmann equation. *Phys. Rev. C* **2018**, *98*, 024912. [CrossRef]
27. Scaria, R.; Sahu, D.; Singh, C.R.; Sahoo, R.; Alam, J.-e. Fluidity of the system produced in relativistic pp and heavy-ion collisions: Hadron resonance gas model approach. *Eur. Phys. J. A* **2023**, *59*, 140. [CrossRef]
28. Acharya, S. et al. [ALICE Collaboration] Evidence of rescattering effect in Pb–Pb collisions at the LHC through production of $K^*(892)^0$ and $\phi(1020)$ mesons. *Phys. Lett. B* **2020**, *802*, 135225. [CrossRef]
29. Singha, S.; Mohanty, B.; Lin, Z.-W. Studying re-scattering effect in heavy-ion collision through K* production. *Int. J. Mod. Phys. E* **2015**, *24*, 1550041. [CrossRef]
30. Andronic, A.; Braun-Munzinger, P.; Stachel, J. Thermal hadron production in relativistic nuclear collisions: The Hadron mass spectrum, the horn, and the QCD phase transition. *Phys. Lett. B* **2009**, *673*, 142–145. [CrossRef]
31. Cleymans, J.; Redlich, K. Chemical and thermal freeze-out parameters from $1A$ GeV to $200A$ GeV. *Phys. Rev. C* **1999**, *60*, 054908. [CrossRef]
32. Chatterjee, S.; Das, S.; Kumar, L.; Mishra, D.; Mohanty, B.; Sahoo, R.; Sharma, N. Freeze-out parameters in heavy-ion collisions at AGS, SPS, RHIC, and LHC energies. *Adv. High Energy Phys.* **2015**, *2015*, 349013. [CrossRef]
33. Cho, S.; Lee, S.H. Reduction of the K^* meson abundance in heavy ion collisions. *Phys. Rev. C* **2018**, *97*, 034908. [CrossRef]
34. Sahu, D.; Tripathy, S.; Pradhan, G.S.; Sahoo, R. Role of event multiplicity on hadronic phase lifetime and QCD phase boundary in ultrarelativistic collisions at energies available at the BNL Relativistic Heavy Ion Collider and CERN Large Hadron Collider. *Phys. Rev. C* **2020**, *101*, 014902. [CrossRef]
35. Karsch, F. Lattice QCD at high temperature and density. In *Lectures on Quark Matter;* Plessas, W., Mathelitsch, L., Eds.; Springer: Berlin/Heidelberg, Germany, 2002; pp. 209–249. [CrossRef]
36. Aoki, Y.; Endrodi, G.; Fodor, Z.; Katz, S.; Szabo, K. The order of the quantum chromodynamics transition predicted by the standard model of particle physics. *Nature* **2006**, *443*, 675–678. [CrossRef]
37. Bazavov, A. et al. [HotQCD Collaboration] Equation of state in (2+1)-flavor QCD. *Phys. Rev. D* **2014**, *90*, 094503. [CrossRef]
38. Borsányi, S.; Fodor, Z.; Hoelbling, C.; Katz, S.D.; Krieg, S.; Ratti, C.; Szabó, K.K. Is there still any T_c mystery in lattice QCD? Results with physical masses in the continuum limit III. *J. High Energy Phys.* **2010**, *2010*, 73. [CrossRef]
39. Borsányi, S.; Fodor, Z.; Hoelbling, C.; Katz, S.D.; Krieg, S.; Szabó, K.K. Full result for the QCD equation of state with 2+1 flavors. *Phys. Lett. B* **2014**, *730*, 99–104. [CrossRef]
40. Andronic, A.; Braun-Munzinger, P.; Stachel, J.; Winn, M. Interacting hadron resonance gas meets lattice QCD. *Phys. Lett. B* **2012**, *718*, 80–85. [CrossRef]
41. Vovchenko, V.; Anchishkin, D.V.; Gorenstein, M.I. Hadron resonance gas equation of state from lattice QCD. *Phys. Rev. C* **2015**, *91*, 024905. [CrossRef]
42. Andronic, A.; Braun-Munzinger, P.; Stachel, J. Hadron production in central nucleus-nucleus collisions at chemical freeze-out. *Nucl. Phys. A* **2006**, *772*, 167–199. [CrossRef]
43. Stachel, J.; Andronic, A.; Braun-Munzinger, P.; Redlich, K. Confronting LHC data with the statistical hadronization model. *J. Phys. Conf. Ser.* **2014**, *509*, 012019. [CrossRef]
44. Muronga, A. Causal theories of dissipative relativistic fluid dynamics for nuclear collisions. *Phys. Rev. C* **2004**, *69*, 034903. [CrossRef]
45. Kouno, H.; Maruyama, M.; Takagi, F.; Saito, K. Relativistic hydrodynamics of quark–gluon plasma and stability of scaling solutions. *Phys. Rev. D* **1990**, *41*, 2903–2911. [CrossRef] [PubMed]
46. Muronga, A. Second order dissipative fluid dynamics for ultrarelativistic nuclear collisions. *Phys. Rev. Lett.* **2002**, *88*, 062302. [CrossRef]
47. Israel, W. Nonstationary irreversible thermodynamics: A causal relativistic theory. *Ann. Phys.* **1976**, *100*, 310–331. [CrossRef]
48. Stewart, J.M. On transient relativistic thermodynamics and kinetic theory. *Proc. R. Soc. Lond. A Math. Phys. Sci.* **1977**, *357*, 59–75. Available online: https://www.jstor.org/stable/79453 (accessed on 22 March 2025).
49. Israel, W.; Stewart, J.M. Transient relativistic thermodynamics and kinetic theory. *Ann. Phys. (N.Y.)* **1979**, *118*, 341–372. [CrossRef]
50. Prakash, M.; Prakash, M.; Venugopalan, R.; Welke, G. Nonequilibrium properties of hadronic mixtures. *Phys. Rep.* **1993**, *227*, 321–366. [CrossRef]
51. Kadam, G.P.; Mishra, H. Dissipative properties of hot and dense hadronic matter in an excluded-volume hadron resonance gas model. *Phys. Rev. C* **2015**, *92*, 035203. [CrossRef]
52. Tiwari, S.K.; Tripathy, S.; Sahoo, R.; Kakati, N. Dissipative properties and isothermal compressibility of hot and dense hadron gas using non-extensive statistics. *Eur. Phys. J. C* **2018**, *78*, 938. [CrossRef]
53. Lokhtin, I.P.; Snigirev, A.M. A model of transverse expansion of the quark gluon fluid with phase transition and hadron spectra in heavy ion collisions. *Phys. Lett. B* **1996**, *378*, 247–254. [CrossRef]

54. Hanus, P.; Mazeliauskas, A.; Reygers, K. Entropy production in pp and Pb–Pb collisions at energies available at the CERN Large Hadron Collider. *Phys. Rev. C* **2019**, *100*, 064903. [CrossRef]
55. Loizides, C.; Kamin, J.; d'Enterria, D. Improved Monte Carlo Glauber predictions at present and future nuclear colliders. *Phys. Rev. C* **2018**, *97*, 054910. [CrossRef]
56. Bleicher, M.; Aichelin, J. Strange resonance production: Probing chemical and thermal freeze-out in relativistic heavy ion collisions. *Phys. Lett. B* **2002**, *530*, 81–87. [CrossRef]
57. Torrieri, G.; Rafelski, J. Strange hadron resonances as a signature of freeze-out dynamics. *Phys. Lett. B* **2001**, *509*, 239–245. [CrossRef]
58. Johnson, S.C.; Jacak, B.V.; Drees, A. Rescattering of vector meson daughters in high-energy heavy ion collisions. *Eur. Phys. J. C* **2001**, *18*, 645–649. [CrossRef]
59. Ilner, A.; Blair, J.; Cabrera, D.; Markert, C.; Bratkovskaya, E. Probing the hot and dense nuclear matter with K^*, $\bar{K}^*$ vector mesons. *Phys. Rev. C* **2019**, *99*, 024914. [CrossRef]
60. Thews, R.L. Quarkonium formation at high energy. *Nucl. Phys. A* **2002**, *702*, 341–345. [CrossRef]
61. Thews, R.L.; Schroedter, M.; Rafelski, J. Enhanced J/ψ production in deconfined quark matter. *Phys. Rev. C* **2001**, *63*, 054905. [CrossRef]
62. Andronic, A.; Braun-Munzinger, P.; Stachel, J.; Stocker, H. Production of light nuclei, hypernuclei and their antiparticles in relativistic nuclear collisions. *Phys. Lett. B* **2011**, *697*, 203–207. [CrossRef]
63. Yang, K.; Xu, X.-M.; Weber, H.J. Cross sections for inelastic meson–meson scattering. *Phys. Rev. D* **2017**, *96*, 114025. [CrossRef]
64. Li, W.-X.; Xu, X.-M.; Weber, H.J. Cross sections for 2-to-1 meson–meson scattering. *Eur. Phys. J. C* **2021**, *81*, 225. [CrossRef]
65. Nendzig, F.; Wolschin, G. Bottomium suppression in PbPb collisions at LHC energies. *J. Phys. G* **2014**, *41*, 095003. [CrossRef]
66. Hoelck, J.; Nendzig, F.; Wolschin, G. In-medium Y suppression and feed-down in UU and PbPb collisions. *Phys. Rev. C* **2017**, *95*, 024905. [CrossRef]
67. Acharya, S. et al. [ALICE Collaboration] Production of charged pions, kaons, and (anti-)protons in Pb–Pb and inelastic pp collisions at $\sqrt{s_{NN}}$ = 5.02 TeV. *Phys. Rev. C* **2020**, *101*, 044907. [CrossRef]
68. Navas, S. et al. [Particle Data Group]. Review of Particle Physics. *Phys Rev D* **2024**, *110*, 030001. [CrossRef]
69. Aggarwal, M.M. et al. [STAR Collaboration] K^{*0} production in Cu+Cu and Au+Au collisions at $\sqrt{s_N N} = 62.4$ GeV and 200 GeV. *Phys. Rev. C* **2011**, *84*, 034909. [CrossRef]
70. Acharya, S. et al. [ALICE Collaboration] Production of the $\rho(770)^0$ meson in pp and Pb–Pb collisions at $\sqrt{s_{\mathrm{NN}}} = 2.76$ TeV. *Phys. Rev. C* **2019**, *99*, 064901. [CrossRef]
71. Abelev, B.I. et al. [STAR Collaboration] Measurements of ϕ meson production in relativistic heavy-ion collisions at the BNL Realtivistic Heavy Ion Collider (RHIC). *Phys. Rev. C* **2009**, *79*, 064903. [CrossRef]
72. Abelev, B.B. et al. [ALICE Collaboration] $K^*(892)^0$ and $\phi(1020)$ production in Pb–Pb collisions at $\sqrt{sNN}$ = 2.76 TeV. *Phys. Rev. C* **2015**, *91*, 024609. [CrossRef]
73. Pradhan, G.S.; Rath, R.; Scaria, R.; Sahoo, R. Exploring the effect of hadron cascade time on particle production in Xe + Xe collisions at $\sqrt{sNN} = 5.44$ TeV using a multiphase transport model. *Phys. Rev. C* **2022**, *105*, 054905. [CrossRef]

Disclaimer/Publisher's Note: The statements, opinions and data contained in all publications are solely those of the individual author(s) and contributor(s) and not of MDPI and/or the editor(s). MDPI and/or the editor(s) disclaim responsibility for any injury to people or property resulting from any ideas, methods, instructions or products referred to in the content.